ICARUS 115, 295–303 (1995)

The Exospheric Systems of Saturn's Rings

W.-H. IP

Max-Planck-Institut fuer Aeronomie, D-37191 Katlenburg-Lindau, FRG

Received June 23, 1994; revised December 5, 1994

Because of collisional interaction with interplanetary meteoroids, the ring system of Saturn is supposedly a major source of neutral gas cloud in the inner saturnian system. We consider some new features brought about by the asymmetric impact geometry of the ring–meteoroid interaction. An assessment is also attempted on the most likely spatial structure and neutral gas number density distribution of the ring exosphere. A meteoroid-impact gas production rate of 5×10^{27} molecules/sec which is a factor of 100 lower than the maximum value previously derived is preferred in the present work. The maximum density of the H_2O molecules in the vicinity of the B ring is about 100 cm^{-3}. Finally, because of gas–surface interaction in the ring environment a thin disc of oxygen molecules might form as one of the major components of the ring exosphere with a density of about 3000 cm^{-3}. This molecular oxygen cloud, if it exists, would in turn supply a flux of oxygen atoms via photodissociation to the orbital region of the icy satellites.

1. INTRODUCTION

Even though the Voyager mission has provided much new information concerning the orbital structure and dynamics of the ring system of Saturn, we still know very little about its evolutionary history and origin. We know, however, that the rings must be subject to continuous impact bombardment by comets and interplanetary meteoroids and that the lifetime and mass distribution of the ring system could therefore be determined by its meteoroid interaction. The recent impact of Comet Shoemaker–Levy 9 at Jupiter demonstrated that large perturbations to the structure of the ring system could result from the sporadic catastrophic encounters of cometary nuclei with the ring particles. It is still to be determined to what degree will such comet–ring collision represent a net mass loss or net gain for the ring system. Compared with this kind of major upheavals with a time interval of a few 10^5 years, the meteoroid influx to the ring system is perhaps no less important. On the basis of different assumptions of the mass flux of the interplanetary meteoroids, several estimates on the "erosion" lifetime (t_e) of the ring system have been made with the values ranging from 10^6 to 10^9 years (see Morfill *et al.* 1983, Connerney and Waite 1984, Ip 1984a).

While the wide range of t_e values given above reflects simply the uncertainties in our knowledge of the meteoroid influx at 10 AU and the resulting impact process with the icy ring particles, it also points to the interesting possibility that the ring system may be relatively young with an age of less than 10^8 years. If true, this finding will lead to another major puzzle: why the ring system is so young in cosmological terms. Was it the result of the fragmentation of an inner icy satellite or the tidal breakup of a large comet (Ip 1988, Dones 1991)? However, this question always returns to the key issue of ring–meteoroid interaction as it is basic to the time scale argument. Since the generation of impact vapor is one of the byproducts of hypervelocity meteoroid collisions, it is important to explore whether any fundamental parameters could be measured from remote observations of the gas emission surrounding the rings. For example, a determination of the hydrogen gas production rate from impact process might tell us what is the effective erosion rate of the ring particles.

A clear picture of the extension and density distribution of the ring atmosphere is also crucial to the understanding of the global distribution of the hydrogen atoms in the whole saturnian system as recently discussed by Shemansky and Hall (1992). The detection of a large quantity of OH with the number density reaching $n(OH) \approx 160$ cm^{-3} at a radial distance of 4.5 R_S (Shemansky *et al.* 1993) has reinforced the view that a comprehensive inventory of the neutral gas environment of the saturnian system is still to be carried out. Another related problem has to do with the origin of the thermal plasma in the inner magnetosphere within a few planetary radii (R_S) distance from the central planet (see Richardson 1992). It is hence useful to reexamine the theoretical models of the ring exosphere incorporating new developments since the work by Ip (1984b) and Pospieszalska and Johnson (1991). In this report we will consider three related topics: (a) the orbital dynamics of the meteoroid-ring collision, (b) the physical consequences of such impact geometry, and finally (c) the possibility of the formation of a

0019-1035/95 $6.00

thin layer of molecular oxygen atmosphere in the vicinity of the ring system.

2. THE ORBITAL DYNAMICS OF METEOROID-RING IMPACTS

Up to now, most of the models of the ring atmosphere were based on the assumption that the emission of the gas particles is azimuthally symmetric around the planet. That is, there are no differences in the production rates between the day-side and night-side regions. However, the meteoroid impact dynamics depend on several factors. First, the original orbital distribution of the interplanetary meteoroids which might be similar to (a) that of the "long-period" (L-P) comets from the distant Oort cloud with isotropic variation in their orbital inclinations or (b) that of the "intermediate-period" (I-P) comets from the Kuiper belt which have relatively small inclinations as in the case of the short-period comets. Second, at collision with the ring particles the pertinent impact speed must be determined by the vectorial sum of the meteoroid velocity and the orbital velocity of the ring particles. When these two dynamical effects are taken into consideration, it can be shown by analytical method (Cuzzi and Durisen 1990) and numerical calculations (Ip unpublished manuscript, 1989) that there exists a strong local time dependence for the emission pattern of the impact vapor.

This particular effect of impact geometry is a combination of the angular distribution of the impact occurrence frequency (f_i) and the impact speed (v_i). for the L-P meteoroids, the f_i value peaks near the dawn side and reaches a dip at the dusk side. This is because of their highly eccentric orbits with aphelion distances being much larger than 10 AU, the incoming particles in retrograde orbits would tend to collide head on with the saturnian system as they intercept the orbit of Saturn. As far as collision with the ring particles is concerned the blockage by the planetary disk will produce a shadow cone projected onto the dusk side of the ring system (see Fig. 1). On the other hand, almost every point at the ring could be reached by objects in prograde orbits. A dawn-to-dusk asymmetry is hence introduced.

In our numerical experiments (Ip unpublished manuscript, 1989) particles emitted from ring particles with an emission velocity of v_e = 27 km sec^{-1} are all in direct orbits and the launch points are found to be distributed nearly uniformly in azimuthal angle. As the v_e value increases, more and more particles will be launched into indirect orbits and the azimuthal symmetry will become more pronounced. Finally, at $v_e \approx 35$ km/sec, only particles in retrograde orbits will be able to reach the ring system and the angular distribution of the launch points in maximum at the dawn side and minimum at the dust side.

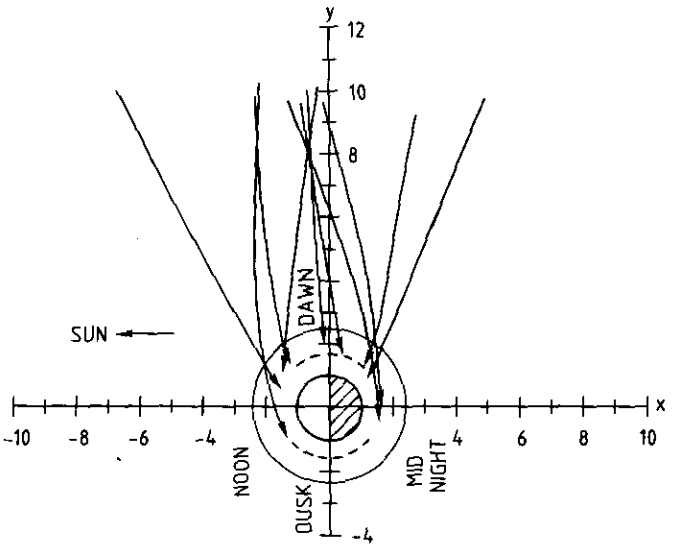

FIG. 1. A schematic view of the geometry of the collisional interaction of long-period comets/meteoroids in retrograde orbits with the ring system. The impacting projectiles tend to approach Saturn in the head-on direction, thus leading to the formation of a shadow cone on the dusk side.

Because of the vectorial relation, $v_i = v_e + v_k$, where v_k is the Keplerian velocity of the ring particle, the impact velocity will be maximal near the midnight and minimal near noon for retrograde meteoroids approaching the ring system in the head-on direction. If the erosion rate ξ_i of the ring particles or the corresponding gas production rate resulting from impact vapor is assumed to be proportional to the impact occurrence frequency and impact kinetic energy, $\xi_i \alpha f_i v_i^2$, the local time variation of ξ_i will have a minimum at the dusk side and a maximum at the predawn sector. For meteoroids in I-P orbits, a similar effect can be found to occur though with a smaller degree of asymmetry. Also, the maximum of ξ_i will be shifted to the local midnight and the minimum to the local noon. As shown in Fig. 2, the maximum-to-minimum ratio is nearly 4 in one numerical run. The introduction of such emission pattern therefore could produce significant deviation from the azimuthally symmetric distributions considered previously by Ip (1984b) and Pospieszalska and Johnson (1991). Such angular variation can be approximated by using the expression: $\xi_i(\phi) \approx 5 + 3 \cos \phi$ where $\phi = 0$ at midnight.

3. RING EXOSPHERE: MODEL STUDIES

Before we proceed with the modeling of the ring atmosphere, it should be noted that the erosion mechanism of icy bodies by hypervelocity collision is still not known in

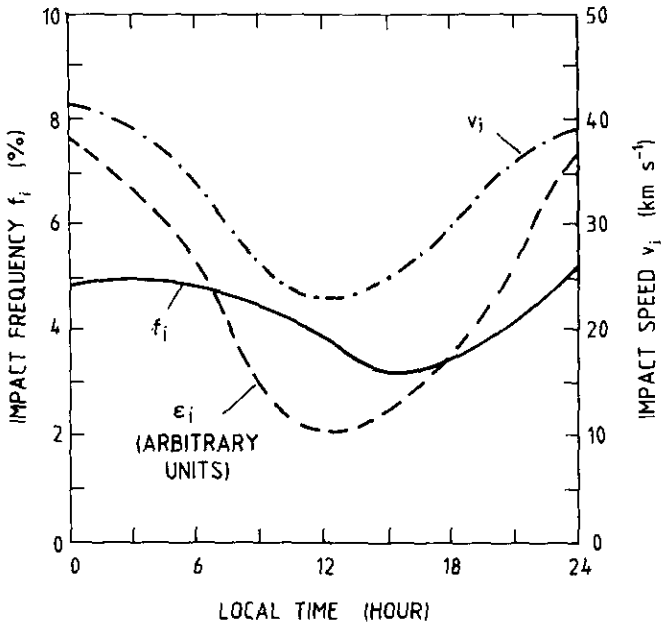

FIG. 2. The local time variations of (a) the ring impact occurrence frequency (f_i), (b) the impact speed (v_i), and (c) the impact erosion rate (ξ_i) for meteoroids in intermediate orbits with aphelion distances less than 20 AU.

detail. For example, it is unclear what would be the mass of the impact vapor (m_v) created by a hyperspeed projectile of mass m_p. Furthermore, the initial temperature (T_o) of the expanding gas generated immediately after impact is not documented for water ice at the relevant impact velocities (20–40 km sec^{-1}). The shock model of hypervelocity collision suggests that upon impact a point explosion is initiated that generates a shock wave propagating through the target material; the compression heats the material to a temperature of about 10^5 K such that a portion of it will be vaporized (Hornung and Drapatz 1981, Morfill and Goertz 1983). For water ice, the initial expansion speed of the impact vapor could thus in principle be as high as 20–30 km sec^{-1} in the shock model. This value, however, appears to be much too high considering that the vapor temperature of micrometeoroid impact was usually given to be about 1000 K (O'Keefe and Ahrens, 1978).

As for the velocity distribution function of the expanding vapor gas, Ip (1984b) applied a Maxwellian velocity distribution to the impact vapor gas particles with the thermal temperature ranging between 100 K and 10,000 K. Pospieszalska and Johnson (1991) followed the experimental measurements of heavy ion sputtering of ices and considered, in addition, an ejected particle energy distribution of the form of $F(E) \propto U/(E + U)^2$, with $U \approx 0.1$ eV. (Note that with $U \approx kT_o$, we have an equivalent vapor temperature of $T_o \approx 1000$ K.) If the initial vapor temperature should be comparable to the sublimation temperature of the target material, a much lower value of T_o (and hence U) would have to be used for water ice instead. Currently, this is perhaps one of the major uncertainties in limiting our ability to model realistically the spatial configuration of the ring exosphere. With this in mind, we shall test a range of the T_o values in our model calculations below.

Approximating the angular asymmetry of the gas emission rate by the local time dependence of the ξ_i value of the I-P meteoroids, the ring exosphere can be constructed by following the numerical scheme outlined in Ip (1984b). Test particles are ejected from the ring plane isotropically according to the Maxwellian velocity distribution with the thermal speed v_{th} assumed to be (a) 2 km sec^{-1}, (b) 3 km sec^{-1}, and (c) 4 km sec^{-1}. For water molecules, the corresponding kinetic energy (U) will be 0.38, 0.86, and 1.52 eV, respectively. The radial positions of the launch points are chosen randomly—but with appropriate account for the radial variation of the ring optical depth—between the outer edge of the A ring at 2.27 R_s and the inner edge of the C ring at 1.23 R_s. At emission each test particle is assigned a weighting factor (f_o). To account for the optical depth effect, every time the test particle crosses the A ring between 2.02 and 2.27 R_s the f value is reduced by a factor of exp $(-0.5/\cos\theta)$; at crossing of the B ring between 2.02 and 1.52 R_s, the f value is reduced by a factor of exp$(-1/\cos\theta)$, where θ is the polar angle of the velocity vector. The trajectory calculation is terminated when one of the following conditions is met:

(a) the particle collides with the planetary surface or

(b) the particle is on a hyperbolic orbit escaping the saturnian system.

Because the dynamical lifetime for most of the particles under consideration is relatively short ($\lesssim 10^5$ sec) the loss due to ionization by the magnetospheric plasma is small.

The model density distributions in the noon–midnight meridional plane are illustrated in Fig. 3. The asymmetric patterns caused by the impact geometry of the interplanetary meteoroids are clearly evident for cases (b) and (c). In case (a) with $V_o \approx 2$ km sec^{-1}, the meteoroid-generated neutral cloud is more closely bound to the ring plane thus obscuring the asymmetric effect (see Fig. 4).

In our model calculations, the number density of the neutral gas cloud is obtained by scaling the total number of test particles employed to the meteoroid impact vapor production rate (Q); see Appendix for details. In the present computations, Q is taken to be 5×10^{27} sec^{-1}, which is approximately 1% the upper limit determined by Northrop and Connerney (1987). There are two reasons for choosing this value. First, reevaluations of the interplanetary meteroid flux at 10 AU solar distance showed that Morfill *et al.* (1983) might have overestimated the

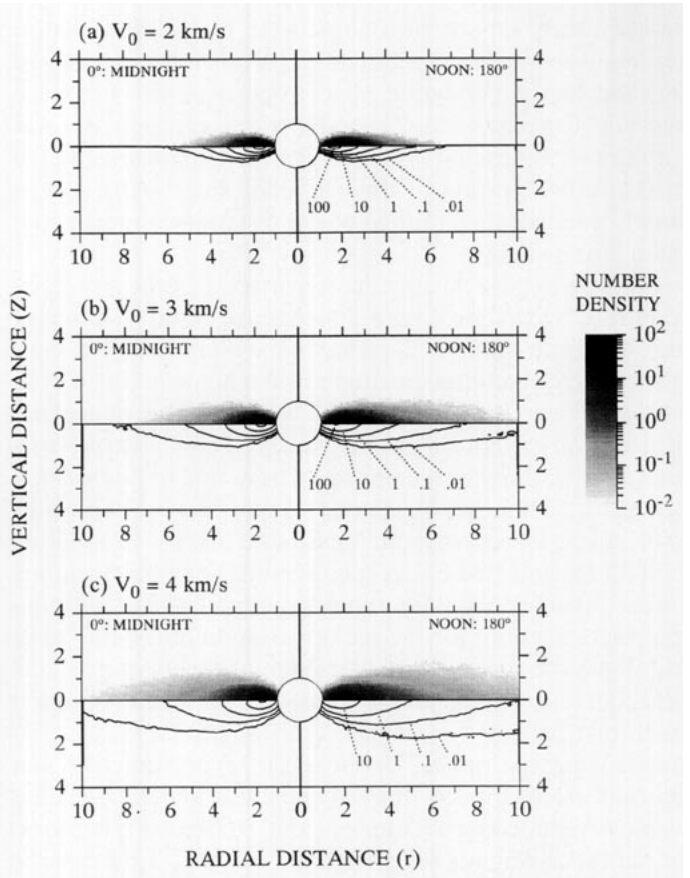

FIG. 3. The cross sections in the noon–midnight meridional plane of the number density distribution of the meteoroid impact-driven neutral cloud from the rings for three different values of the initial thermal speed: (a) $V_0 = 2$ km sec^{-1}, (b) $V_0 = 3$ km sec^{-1}, and (c) $V_0 = 4$ km sec^{-1}. Note that the initial velocity distribution at emission from the ring plane is assumed to be Maxwellian.

relevant meteoroid influx by a factor of 10–100 (Ip 1984a, Haff and Eviatar 1986). Since the Morfill *et al.* value was the basis for the maximum Q value used by Northrop and Connerney (1987), a proportional reduction in the impact vapor production rate therefore would be required. Next, of equal importance, a significant fraction of the impact vapor might be ionized at production. According to Grün and Reinhard (1981) the degree of ionization could be more than 60% for impacting meteoroids with size <100 μm under certain circumstances. The newly produced ions are picked up by the planetary magnetic field and the motion of the ionized cloud is tied to the corotating magnetic field without following ballistic orbits. As a result, in the present calculations the neutral cloud density associated with the ring system ($n \approx 10$ cm^{-3} at $r \approx 2.5\ R_s$) would be considerably smaller than the value given by Pospieszalska and Johnson (1991) and other authors.

Another factor in reducing the density of the ring exosphere has to do with the actual value of the expansion velocity. In Fig. 3 we have shown the neutral density distributions for cases with $V_o \approx 2$–4 km sec^{-1} so that the asymmetric impact emission effects could be better observed. Thermal speeds of this range imply vapor temperature 4.4×10^3 and 1.6×10^4 K for H_2O molecules. A more suitable value may be $\approx 10^3$ K (and $U \approx 0.1$ eV) as indicated by laboratory studies (O'Keefe and Ahrens 1978). According to these assessments, the "minimal" model as described by case (a) in Fig. 3 could probably be closest to the actual structure of the primary ring exosphere.

This is, however, not to say that the rings could not eject neutral atoms or molecules into far-flung orbits. If a layer of dense neutral gas could be built up near the rings with H_2O, OH, H_2, and/or O_2 as the main components, it could serve as a reservoir of atomic hydrogen and oxygen fragments of significant excess energy (≈1–2 eV) as a result of photodissociation. Furthermore, the photodissociation of O_2 molecules ($O_2 + h\nu \rightarrow O(^3P) + O(^1D)$) leads to oxygen atoms carrying an excess energy of 1.3 eV (Huebner and Carpenter 1979). The secondary ring exosphere which is formed of the atomic oxygen fragments would thus be similar to the model distribution depicted by case (b) or (c) with one important difference, namely, the asymmetric pattern should be oriented in the opposite direction because photodissociation would be quenched in the planetary shadow.

The potential buildup of an oxygen atmosphere of the rings can be described in the following way. To begin with, the atomic fragments such as H, O, and OH, when they collide with the icy ring particles, could either stick to the surface or rebound immediately. The component which is attached to the ring surface would subsequently be lost via chemical reactions. With surface reactions like

$$OH + OH \rightarrow H_2O + O \quad (1)$$

and

$$O + OH \rightarrow O_2 + H, \quad (2)$$

a monolayer of O_2 molecules could form. While the H_2O molecules tend to recondense the presence of a monolayer of oxygen molecules could probably inhibit the further absorption of O_2 very effectively.

The minimum production rate of the atomic oxygen can be derived by consideration of the photodissociation of the H_2O vapor from meteoroid impact. At a solar distance of 10 AU, the photodissociation time scale for the reaction

$$H_2O + h\nu \rightarrow H + OH \quad (3)$$

is on the order of $\tau' \approx 10^7$ sec at solar minimum (Huebner and Carpenter 1979). For an orbital lifetime of about 15 hr

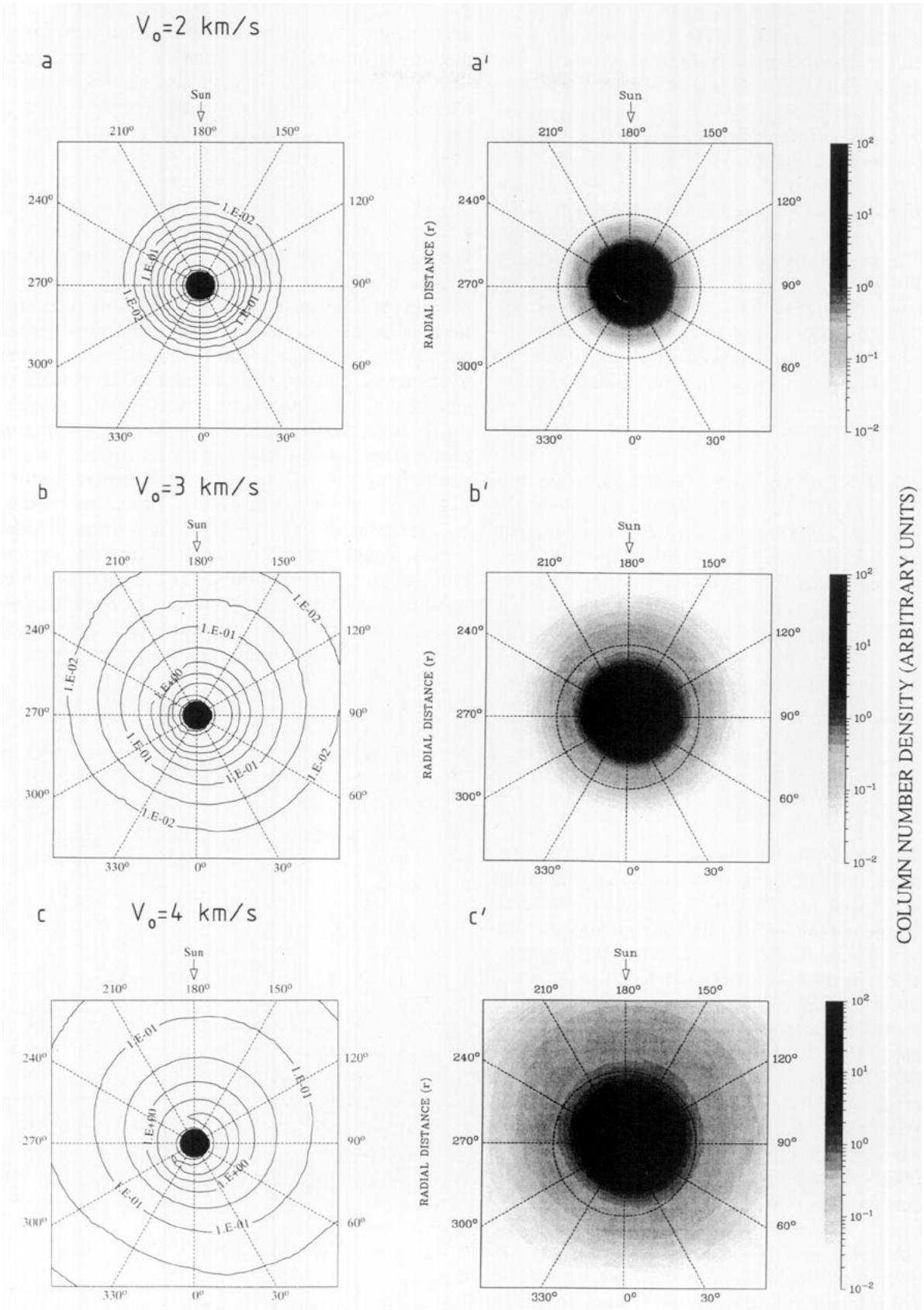

FIG. 4. Projections of the column density of the ring atmospheres on the ring plane for different values of the initial thermal speed: (a) V_o = 2 km sec^{-1}, (b) V_o = 3 km sec^{-1}, and (c) V_o = 4 km sec^{-1}.

for the H_2O molecules emitted away from the ring plane, the probability of creating an oxygen atom during the ballistic flight of the H_2O molecule is consequently $P \approx 5.3 \times 10^{-3}$. After recycling by the ring interaction, the oxygen molecules so formed will be stored in a disc-like region embedding the ring plane. This atmospheric disc could be characterized as having the same radial dimension covering the A and B rings and a vertical half thickness given as $h \approx (V_{th}/V_k)\langle r\rangle$ where V_k is the Keplerian velocity of the ring particles at an average radial distance of $\langle r\rangle$, and V_{th} is the thermal velocity of O_2 at a (ring surface) temperature of about 100 K. With $V_k \approx 18$ km/sec, $V_{th} \approx 0.3$ km/second, and $\langle r\rangle \approx 1.9\ R_s$ we have $h \approx 1900$ km. The average number density of oxygen molecules stored in this reservoir can then be approximated as

$$\langle n(O_2)\rangle \approx PQ(H_2O)\tau''/V, \tag{4}$$

where $V \approx 2.15 \times 10^{29}$ cm^3 and τ'' is the corresponding loss time scale of O_2. If the plasma density along the magnetic field lines connected with the ring plane is small ($\eta_i \lesssim 100$ cm^{-3}) such that electron impact ionization and dissociation as well as ion–molecule reactions are not important, τ'' can be equated to the photodissociation time scale of the oxygen molecules of 2.4×10^7 sec. With Q and V as estimated above we have

$$\langle n(O_2)\rangle \approx 2.9 \times 10^3 \left(\frac{5 \times 10^{27}}{Q}\right)\left(\frac{7.6 \times 10^{-4}}{P}\right)\left(\frac{2.4 \times 10^7}{\tau''}\right) \text{cm}^{-3}. \tag{5}$$

While this is a significant value when compared with the number densities in the neutral cloud environment of the saturnian system (e.g., $n(OH) \approx 160$ cm^3 at $r \approx 4.5\ R_s$ according to Shemansky *et al.* (1993)), this oxygen number density could be further increased by invoking electron impact dissociation of the H_2O molecules at $r > 2.27\ R_s$, or the introduction of the assumption that a significant fraction of the meteoroid vapor is in the form of O_2. For example, if the relative yields of O_2 vs H_2O for energetic (MeV) charged particle sputtering on water ice (Johnson *et al.* 1989) are a reasonable approximation, the relative abundance of the oxygen molecules entrained in the meteoroid impact vapor cloud could be as much as 0.01–0.1. This source mechanism alone would permit an enhancement of $\langle n(O_2)\rangle$ to a level of 6×10^3 to 6×10^4 molecules cm^{-3}. In this way, the surface reaction of the oxygen atoms and the OH radicals after collisional absorption by ring particles would necessarily lead to the formation of a major ring neutral cloud enriched in O_2 (and H_2). Though it is doubtful that the sputtering results could be directly applied to the situation of hypervelocity meteoroid impact (R. E. Johnson private communication, 1994), this makes it even more interesting to test this hypothesis by means of remote-sensing observations, say, during the saturnian ring edge-on opportunity in 1995.

4. DISCUSSION

In this work we have made an attempt to assess the structure of the neutral cloud according to recent developments in related topics. We find that several new notions might have to be added to our general understanding of the saturnian neutral cloud system. First, the asymmetric pattern of ring–meteoroid interaction discussed by Cuzzi and Durisen (1990) and Ip (unpublished manuscript, 1989) could probably also show up in the distribution of the meteoroid impact-driven neutral cloud made up of H_2O, OH, O_2, O, H_2, and H. As the initial expansion velocity of the impact water vapor should be on the order of 1–2 km sec^{-1}, the primary ring atmosphere would be tightly confined to the ring system with only very limited contribution to the neutral gas environment beyond the orbit of Mimas. The dependence of the ring gas cloud on the emission speed can be seen in Figs. 4 and 5 for the radial variation of the integrated column

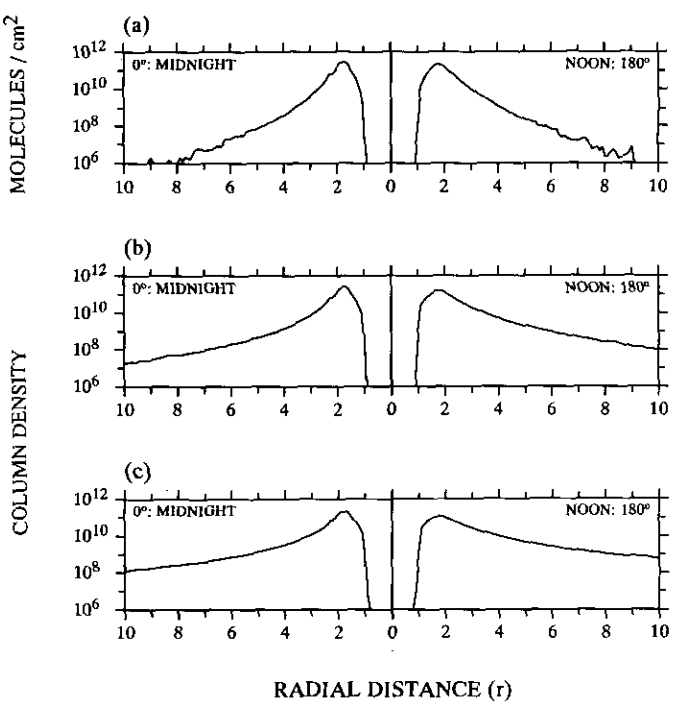

FIG. 5. Radial distribution of the integrated column density of the H_2O molecules ejected from the Saturnian rings: (a) $V_o = 2$ km sec^{-1}, (b) $V_o = 3$ km sec^{-1}, and (c) $V_o = 4$ km sec^{-1}.

density of the ejected water molecules. If a significant amount of oxygen molecules is stored in the vicinity of the ring plane, photodissociation would create a population of oxygen atoms reaching as far as the orbit of Dione and beyond. Because of its photolytic origin the atomic oxygen cloud so formed would display an asymmetric configuration just opposite to the meteoroid impact-driven component.

The long-standing conflict between the ring neutral cloud source mechanism and thermal plasma models (Richardson, 1987, 1992) may be partially resolved at the expense of the effective source strength of the ring atmosphere. For example, by opting for a gas production rate of 5×10^{27} molecules sec^{-1} we would probably be able to accommodate the constraint set by the thermal plasma observations as far as the heavy ions are concerned. However, with the current (minimal) model we are unable to shed any new light on the radial distribution of hydrogen atoms as deduced by Shemansky and Hall (1992) from the Voyager Ultraviolet Spectrometer observations. According to these authors, the number density of H atoms should increase inward until reaching the planetary surface. Even though it has recently been shown that the solar radiation pressure effect could significantly modify the atomic hydrogen torus of Titan to the extent that the distribution of the associated neutral cloud on the dawn side should be pushed radially inward filling the whole region between the ring system and Titan's orbit (Smyth and Marconi 1993, Ip 1994), the observed variation remains unexplained. It is possible that other process(es) unique to the saturnian system could be at work here. One mechanism proposed by Shemansky and Smith (1982) requires that an intense flux of hydrogen atoms be emitted from Saturn's day side exosphere as a result of impact dissociation of the H_2 molecules by a population of suprathermal electrons. This particular process has not been examined in detail in the context of ring–exosphere interaction.

Another problem to be investigated concerns the possible collisional interaction of the E-ring icy particles of micrometer size with the main ring system (Baum *et al.* 1980). From numerical calculations of the orbital motion of charged dust particles Horanyi *et al.* (1992) and Hamilton and Burns (1994) showed that within a narrow size range near 1 μm, the dust particles emitted from Enceladus could be quickly perturbed into orbits crossing the ring system. A fraction of the E ring particles might thus collide with the main rings, generating impact ejecta and vapor. Since the impacting particle flux from the E ring could be significant in comparison with the interplanetary meteoroid flux according to the estimate by Hamilton and Burns (1993), this effect is not to be overlooked and will be examined in the future.

Finally, the asymmetric pattern of the meteoroid–ring interaction is still not known very accurately because of the uncertainty in the orbital distribution of interplanetary particles in the outer Solar System. However, the basic features as described here should nevertheless hold. Future observations by groundbased and spaceborne telescopes as well as the measurements to be made by Cassini will provide many important insights to this intriguing exospheric system.

APPENDIX

In our calculations, the number densities of the gas particles in different radial and angular positions are computed in the following way. First, the saturnian system is divided into grid points in a cylindrical coordinate system with $r_i = i\Delta r$, $z_j = j\Delta z$, and $\phi_k = k\Delta\phi$ in the azimuthal direction. We have $\Delta r = \Delta z = 0.1\ R_s$ and $\Delta\phi = 3°$. Second, the Keplerian motion of the test particle after emission from a launch point will be followed by using a Runge–Kutta fourth-order integration subroutine with a fixed time step Δt. At the starting point, a weight factor f_o will be assigned according to the initial radial distance:

(a) $f_o = 0.10$ if $1.214\ R_s < r_o < 1.530\ R_s$ [C ring]
(b) $f_o = 1.0$ if $1.530\ R_s < r_o < 1.95\ R_s$ [B ring]
(c) $f_o = 0.06$ if $1.95\ R_s < r_o < 2.21\ R_s$ [B ring]
(d) $f_o = 0.50$ if $2.21\ R_s < r_o < 2.26\ R_s$ [A ring].

At time step t_n ($= n\Delta t$), the position of the test particle will be checked and binned into appropriate volume element (i, j, k) in which it is located. The corresponding weight factor f_n will be registered and added to the sum value of $F(i, j, k)$.

At the crossing of the ring plane at time step t_m, the absorption loss of the test particle (which numerically represents an assemblage of gas molecules) will be simulated by a reduction of the weight factor by a factor of $\eta = \exp(-\tau/\cos\theta)$ where θ is the polar angle of the velocity vector; that is, $f_m = \eta f_{m-1}$. Note that $\tau = 0.5$ for crossing of the A ring between 2.02 and 2.27 R_s and $\tau = 1$ for crossing of the B ring between 1.52 and 2.02 R_s.

The particle motion is first traced through one orbital period with the radial positions of the ascending node (r_u) and descending node (r_d) marked. (Because of the assumption of mirror symmetry at the ring plane, the ascending nodes are all located at the launch points). The reduction factor η_u at r_u is then computed as well as η_d if $1.52\ R_s < r_d < 2.27\ R_s$ ($\eta_d = 1$ by default).

If no other loss processes such as electron impact ionization and/or photoionization are involved, the accounting could be highly simplified. For continuous returns to the same ring plane crossing points, we can see that the cumulative sum values $[F(i, j, k)]$ at individual bins in the upward leg of the trajectory will be

$$F(i, j, k) = 1 + \eta_u\eta_d/(1 - \eta_u\eta_d) \tag{A1}$$

and that of the downward leg by

$$F(i, j, k) = n_u/(1 - \eta_u\eta_d). \tag{A2}$$

With this information we could repeat the orbital calculation once more and accumulate the F values at pertinent grids along the particle trajectory. If we apply the same procedure to a total of N_T test particles

considered in a numerical run, the "virtual" number density in the volume element (i, j, k) will be

$$FF(i, j, k) = \sum_{N=1}^{N_r} F(i, j, k). \tag{A3}$$

In the Monte Carlo calculations, a total of N launch points are chosen with their initial radial distances (r_0) randomly selected between 1.214 and 2.26 R_s and the initial azimuthal angles ϕ_0 fixed to be zero. At each launch point, a total of M test particles will be emitted (e.g., $N_r = N \times M$). The initial particle speed (v_e) in the comoving frame of the parent ring particle in Keplerian motion is determined from a random number generator subroutine characterized by Maxwellian distribution. The angular orientation of the velocity vector is assumed to be isotropic. That is, we have neglected the optical depth effect due to the finite thickness of the ring system. The initial weight factors (f_0) of the $N \times M$ test particles will be summed together (e.g., $FF_0 = \sum f_0$). As we shall see later the parameter FF_0 plays a key role in the conversion of the "virtual" number densities obtained in the model calculations to absolute values with a given gas emission rate (Q) of the ring system.

To simulate the anisotropic pattern of the azimuthal distribution of the emission points as a result of the meteoroid–ring interaction, the following numerical scheme is developed. That is, we define a new parameter;

$$\xi_l = 5 + 3 \cos(\phi_l), \tag{A4}$$

where $\phi_l = l\Delta\phi$ and $\Delta\phi = 3°$. Rotational transformations of the three-dimensional matrix of $FF(i, j, k)$ obtained before are then made in angular steps of $\Delta\phi$. If the new values of the density matrix after the rotational transformation by an azimuthal angle of $\phi_l = l\Delta\phi$ are denoted as $FF_l^*(i, j, k)$, a summation is carried out for all transformed values to obtain the cumulative matrix,

$$FFF(i, j, k) = \sum_{l=1}^{120} \xi_l FF_l^*(i, j, k). \tag{A5}$$

By the same token, a cumulative weighting factor will also be defined as

$$FFF_0 = \sum_{l=1}^{120} \xi_l FF_0. \tag{A6}$$

Under steady-state condition, the "virtual" gas emission rate in our model calculations is given by $q = FFF_0/\Delta t$. If the ratio between Q (the assumed gas emission rate of the ring system) and q is ψ, the absolute value of the number densities in different grid points can be obtained by using the expression

$$n(i, j, k) = \psi FFF(i, j, k)/V(i, j, k), \tag{A7}$$

where the volume element in cgs units at grid point (i, j, k) is defined as

$$V(i, j, k) = \pi(r_{K+1}^2 - r_K^2)\Delta z/120, \tag{A8}$$

noting that we have added all the particle points into the upper half of the system because of the assumption of mirror symmetry.

In our computations, $N = 100$, $M = 1000$, $FF_0 = 4.7 \times 10^4$, $FFF_0 = 2.82 \times 10^7$, $\Delta t = 75.5$ sec, hence $q = 3.73 \times 10^5$ launches/sec.

ACKNOWLEDGMENTS

I thank R. E. Johnson and an anonymous referee for useful comments and suggestions and Douglas Hamilton for a stimulating discussion on the E ring dynamics.

REFERENCES

Baum, W. A., T. Kreidl, J. A. Westphal, G. E. Danielson, P. K. Seidelmann, D. Pascu, and D. G. Currie 1981. Saturn's E ring. I. CCD observations of March 1980. *Icarus* **47**, 84–96.

Connerney, J. E. P., and H. Waite 1984. New model of Saturn's ionosphere with an influx of water from their rings. *Nature* **312**, 136–138.

Cuzzi, J. N., and R. H. Durisen 1990. Bombardment of planetary rings by meteoroids: General formulation and effects of Oort cloud projectiles. *Icarus* **84**, 467–501.

Dones, L. 1991. A recent origin for Saturn's rings? *Icarus* **92**, 194–203.

Grün, E., and R. Reinhard 1981. Ion-electron pair production by the impacts of cometary neutrals and dust particles on the Halley probe shield. *Cometary Halley Probe Plasma Environment*, ESA SP-155, pp. 7–21.

Haff, P. K., and A. Eviatar 1986. Micrometeoroid impact on planetary satellites as a magnetospheric mass source. *Icarus* **66**, 258–269.

Hamilton, D. P., and J. A. Burns 1993. OH in Saturn's rings. *Nature* **365**, 498.

Hamilton, D. P., and J. A. Burns 1994. Origin of Saturn's E ring: Self-substained, naturally, *Science* **264**, 550–553.

Horanyi, M., J. A. Burns, and D. P. Hamilton 1992. The dynamics of Saturn's E ring particles, *Icarus* **97**, 248–259.

Hornung, K., and S. Drapatz 1981. Residual ionization after impact of large dust particles. *Cometary Halley Probe Plasma Environment*, ESA SP-155, p. 23.

Huebner, W. F., and C. W. Carpenter 1979. *Solar Photo Rate Coefficients*. Los Alamos National Lab. Informal Report LA-8085-MS.

Ip, W.-H. 1984a. Ring torque of Saturn from interplanetary meteoroid impact. *Icarus* **60**, 547–552.

Ip, W.-H. 1984b. The ring atmosphere of Saturn: Monte Carlo simulations of the ring source model. *J. Geophys. Res.* **89**, 8843–8849.

Ip, W.-H. 1988. An evaluation of a catastrophic fragmentation origin of the Saturnian ring system. *Astron. Astrophys.* **199**, 340–342.

Ip, W.-H. 1995. The Asymmetric Distribution of Titan's Atomic Hydrogen Cloud as a Function of Local Time. Submitted for publication

Johnson, R. E., M. K. Pospieszalska, E. C. Sittler, Jr., A. F. Cheng, L. J. Lanzerotti, and E. M. Sieveka 1989. The neutral cloud and heavy ion inner torus at Saturn. *Icarus* **77**, 311–329.

Morfill, G. E., and C. K. Goertz 1983. Plasma clouds in Saturn's rings. *Icarus* **55**, 111–123.

Morfill, G. E., E. Grün, C. K. Goertz, and T. V. Johnson 1983. On the evolution of Saturn's "spokes": Theory. *Icarus* **53**, 230–235.

O'Keefe, J. D., and T. J. Ahrens 1978. Impact-driven energy partitioning, melting, and vaporization on terrestrial planets. *Proc. Lunar Sci. Conf. 8th* 3357–3374.

Pospieszalska, M. K., and R. E. Johnson 1991. Micrometeorite erosion of the main rings as a source of plasma in the inner Saturnian plasma torus. *Icarus* **93**, 45–52.

Northrop, T. G., and J. E. P. Connerney 1987. A micrometeorite erosion model and the age of Saturn's rings. *Icarus* **70**, 124–137.

RICHARDSON, J. D. 1987. Limits on the extent of Saturn's hydrogen cloud. *Geophys. Res. Lett.* **14,** 999–1002.

RICHARDSON, J. D. 1992. A new model for plasma transport and chemistry at Saturn. *J. Geophys. Res.* **97,** 13705–13713.

SHEMANSKY, D. E., AND D. T. HALL 1992. The distribution of atomic hydrogen in the magnetosphere of Saturn. *J. Geophys. Res.* 4143–4161.

SHEMANSKY, D. E., AND G. R. SMITH 1982. Whence comes the "Titan" hydrogen torus? *EOS Trans. AGU* **63,** 1019.

SHEMANSKY, D. E., P. MATHESON, D. T. HALL, H.-Y. HU, AND M. TRIPP 1993. *Nature* **363,** 329.

SMYTH, W. H., AND M. L. MARCONI 1993. The nature of the hydrogen tori of Titan and Triton, *Icarus* **101,** 18–32.